J. Opt. A: Pure Appl. Opt. **11** (2009) 105206 (6pp) doi:10.1088/1464-4258/11/10/105206

Extraction of the anisotropic dielectric properties of materials from polarization-resolved terahertz time-domain spectra

E Castro-Camus[1] **and M B Johnston**[2]

[1] Centro de Investigaciones en Óptica A.C., Loma del Bosque 115, Lomas del Campestre, León, Guanajuato 37150, Mexico
[2] Clarendon Laboratory, Department of Physics, University of Oxford, Parks Road, Oxford OX1 3PU, UK

E-mail: enrique@cio.mx

Received 3 June 2009, accepted for publication 16 July 2009
Published 14 August 2009
Online at stacks.iop.org/JOptA/11/105206

Abstract
The anisotropic complex dielectric properties of materials in the terahertz band is a topic that has attracted considerable attention recently in the fields of physics, chemistry and biochemistry. The mathematical formalism for analysing polarization-resolved terahertz time-domain data is presented, and particular cases including birefringence, optical activity and circular dichroism are discussed.

Keywords: terahertz, ultra-fast, photoconductive, polarization, dichroism, birefringence, quartz

(Some figures in this article are in colour only in the electronic version)

1. Introduction

The development of techniques to generate [1–3] and detect [4, 5] sub-picosecond radiation transients coherently has allowed spectroscopists to access the far-infrared region of the spectrum with unprecedented sensitivity. Based on those early developments, the technique known as terahertz time-domain spectroscopy (THz-TDS) has evolved dramatically and matured [6, 7] over the last 25 years. For example terahertz emitters [8–13] and detectors [14–18] have improved significantly as a result of recent advances in semiconductor fabrication. Until recently, for various reasons, very little attention has been given to the polarization-dependent properties of materials in the terahertz regime, mainly owing to the lack of appropriate spectroscopic technology. Yet in recent years several groups have designed and fabricated polarization sensitive detectors [19–21] that are capable of measuring the full transverse time-dependent terahertz waveform. Furthermore, polarization-related optical elements such as waveplates [22], prisms [23] and polarizers [24] for the terahertz band have been reported. As a result of advances in polarization-resolved THz-TDS, studies of the polarization-dependent terahertz properties of materials are now emerging. In particular there have been reports of the anisotropy of metamaterials [25], biomolecules [26] and inorganic crystals [27] at terahertz frequencies.

The concept of polarization is well defined for plane monochromatic waves [28] in most optics and electromagnetism textbooks. In this paper the formalism for broadband polarization analysis and the equations for extracting polarization-dependent properties from terahertz time-domain spectra are presented. Additionally some convenient graphical representations of polarization for broadband pulses are suggested.

2. Polarization of broadband pulses

In THz-TDS the data directly acquired from the experimental setup are the time-dependent electric field waveform. For analysis purposes, it is convenient to Fourier transform these

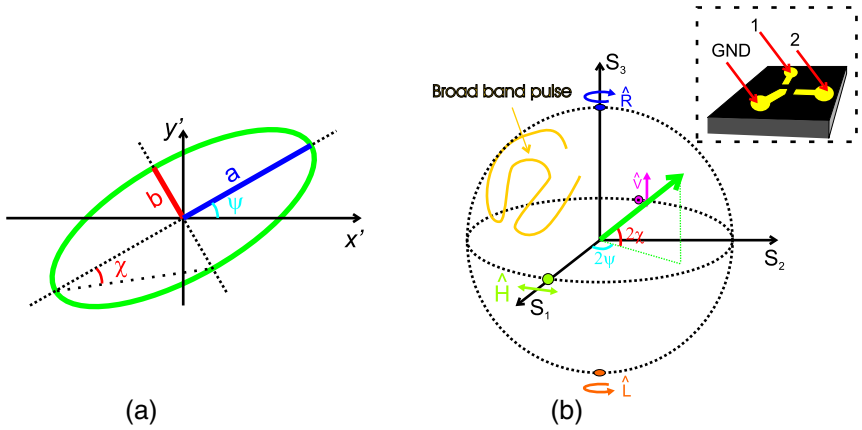

Figure 1. (a) Schematic showing the angles ψ and χ on a polarization ellipse. (b) A schematic of a Poincaré sphere showing how each polarization state is parametrized by ψ and χ. The states $\hat{\mathbf{H}}$, $\hat{\mathbf{V}}$, $\hat{\mathbf{R}}$ and $\hat{\mathbf{L}}$ are indicated on the sphere. A trajectory (yellow) on the surface is the representation of a broadband pulse, the points of the trajectory are the polarization states for each frequency. The inset shows a diagram of the three-contact polarization sensitive detector from [19], there are two numbered contacts (1 and 2) that measure the electric field in the horizontal and vertical directions respectively when referenced to the third common contact (GND).

data to obtain a frequency-dependent spectrum. Polarization, in this case, is *not* a single state, but a collection of states defined for each frequency component present in the broadband pulse. The Jones representation [29] which consists of a two-dimensional complex vector is analytically expressed as

$$\mathbf{j}_{\mathrm{THz}}(\omega) = \begin{pmatrix} \mathcal{E}^{[x']}(\omega)\, \mathrm{e}^{\mathrm{i}\phi^{[x']}(\omega)} \\ \mathcal{E}^{[y']}(\omega)\, \mathrm{e}^{\mathrm{i}\phi^{[y']}(\omega)} \end{pmatrix} \tag{1}$$

where x' and y' refer to orthogonal components on the plane transverse to the direction of propagation of the wave and $\mathcal{E}^{[k]}$ and $\phi^{[k]}$ ($k = x', y'$) are the amplitudes and phases of the Fourier transforms, respectively. The polarizations of the electromagnetic wave can be fully parametrized by

$$\psi(\omega) = \frac{1}{2}\arctan\left[2\frac{\mathcal{E}^{[x']}(\omega)\mathcal{E}^{[y']}(\omega)}{(\mathcal{E}^{[x']}(\omega))^2 - (\mathcal{E}^{[y']}(\omega))^2}\cos(\Delta(\omega))\right] \tag{2}$$

$$\chi(\omega) = \frac{1}{2}\arcsin\left[2\frac{\mathcal{E}^{[x']}(\omega)\mathcal{E}^{[y']}(\omega)}{(\mathcal{E}^{[x']}(\omega))^2 + (\mathcal{E}^{[y']}(\omega))^2}\sin(\Delta(\omega))\right] \tag{3}$$

where $\Delta(\omega) = \phi^{[y']}(\omega) - \phi^{[x']}(\omega)$, ψ is the angle between the major axis of polarization with respect to x' (as illustrated in figure 1(a)) and χ is an auxiliary angle related to the ellipticity ϵ by

$$|\tan\chi(\omega)| = \epsilon(\omega) = \frac{b(\omega)}{a(\omega)} \tag{4}$$

with a and b being the major and minor axes to the polarization ellipse (see figure 1(a)). Notice that χ carries the ellipticity information as well as the handedness. Let $\epsilon_\pm(\omega) = \tan\chi(\omega)$ be the *signed ellipticity*, which is a value that measures the ellipticity and the handedness.

Notice that $\epsilon_\pm(\omega) = 0$ if

$$\Delta(\omega) = m\pi \qquad \text{for } m = 0, \pm1, \pm2, \ldots, \tag{5}$$

which means that the polarization state at frequency ω is linear if the phase difference between its components is an integer multiple of π. Similarly $\epsilon_\pm(\omega) = (-1)^m$ if

$$\Delta(\omega) = (2m+1)\frac{\pi}{2} \qquad \text{for } m = 0, \pm1, \pm2, \ldots, \tag{6}$$

which are the right $\epsilon_\pm(\omega) = 1$ and left $\epsilon_\pm(\omega) = -1$ circular states that occur when the phase difference is a semi-integer multiple of π.

One way of representing an electromagnetic wave geometrically is using a point on the *Poincaré sphere*, which is a subspace of *Stokes' parameter space* [28]. If only the polarization of the electromagnetic wave is of interest (not paying attention to the amplitude) a unit Poincaré sphere (figure 1) can be used as a convenient graphical representation. While for monochromatic waves the state of polarization is fully described by a single point, a broadband pulse will be represented as a trajectory (figure 1(b)) on the sphere. This trajectory can be parametrized in frequency as follows

$$S_1(\omega) = \cos 2\chi(\omega)\cos 2\psi(\omega) \tag{7}$$

$$S_2(\omega) = \cos 2\chi(\omega)\sin 2\psi(\omega) \tag{8}$$

$$S_3(\omega) = \sin 2\chi(\omega), \tag{9}$$

where S_1, S_2 and S_3 are the coordinates in *Stokes' space*.

There are some cases of unit Jones vectors that form orthonormal bases of the polarization space. Some of these are of particular interest and will be used in the rest of this paper:

Jones vector	Label	Name of state
$(1, 0)$	$\hat{\mathbf{H}}$	Horizontal
$(0, 1)$	$\hat{\mathbf{V}}$	Vertical
$(1/\sqrt{2}, -\mathrm{i}/\sqrt{2})$	$\hat{\mathbf{R}}$	*Dextrogyre*
$(1/\sqrt{2}, \mathrm{i}/\sqrt{2})$	$\hat{\mathbf{L}}$	*Levogyre*

Notice that $\hat{\mathbf{H}}$ and $\hat{\mathbf{V}}$ represent the linearly polarized states in the x' and y' directions, respectively, and that $\hat{\mathbf{R}}$ and $\hat{\mathbf{L}}$ are the circular polarization states for the two different handednesses. It is also important to point out that $\hat{\mathbf{H}} \cdot \hat{\mathbf{V}}^* = \hat{\mathbf{R}} \cdot \hat{\mathbf{L}}^* = 0$

and $\hat{\mathbf{H}}\cdot\hat{\mathbf{H}}^* = \hat{\mathbf{V}}\cdot\hat{\mathbf{V}}^* = \hat{\mathbf{R}}\cdot\hat{\mathbf{R}}^* = \hat{\mathbf{L}}\cdot\hat{\mathbf{L}}^* = 1$, and therefore these pairs of Jones vectors form two orthonormal bases for the space of polarizations. These vectors are also graphically represented in figure 1. The following equations can be used to convert vectors expressed in these two particular bases:

$$\hat{\mathbf{H}} = \frac{1}{\sqrt{2}}(\hat{\mathbf{R}} + \hat{\mathbf{L}}), \tag{10}$$

$$\hat{\mathbf{V}} = \frac{\mathrm{i}}{\sqrt{2}}(\hat{\mathbf{R}} - \hat{\mathbf{L}}), \tag{11}$$

$$\hat{\mathbf{R}} = \frac{1}{\sqrt{2}}(\hat{\mathbf{H}} - \mathrm{i}\hat{\mathbf{V}}), \tag{12}$$

$$\hat{\mathbf{L}} = \frac{1}{\sqrt{2}}(\hat{\mathbf{H}} + \mathrm{i}\hat{\mathbf{V}}). \tag{13}$$

3. Analysis of polarization-resolved time-domain data

Fast and insightful analysis of physical problems relies heavily upon the correct choice of coordinate systems. An appropriate coordinate system reduces the equations describing them to simple (or relatively simple) expressions that can be solved analytically or numerically. Polarization-resolved THz-TDS is no exception. In order to simplify the analysis of experimental data measured using this technique it is important to decompose the measured wave in the polarization base corresponding to the *eigenwaves* of the system under study. For example, the eigenwaves of a uniaxial birefringent crystals are the two linearly polarized states, which propagate at different speeds.

The photoconductive receiver presented in [19] measures simultaneously two orthogonal components of the electric field, for convenience from now on x' (y') and therefore $\hat{\mathbf{H}}$ ($\hat{\mathbf{V}}$) will refer to the direction of the electric field measured by contact 1 (2) of the photoconductive receiver as shown in the inset of figure 1. The electric field directly measured by the photoconductive detector is, therefore, naturally written in the $\hat{\mathbf{H}}$, $\hat{\mathbf{V}}$ base. Of course, as stated earlier, the acquired data can be reexpressed in other bases if it is convenient for data analysis purposes. For instance, using equations (1), (10) and (11) in the circular base as

$$\begin{aligned}\mathbf{j}_{\mathrm{THz}}(\omega) &= \frac{1}{\sqrt{2}}(\mathcal{E}^{[x']}(\omega)\,\mathrm{e}^{\mathrm{i}\phi^{[x']}(\omega)} + \mathrm{i}\mathcal{E}^{[y']}(\omega)\,\mathrm{e}^{\mathrm{i}\phi^{[y']}(\omega)})\hat{\mathbf{R}} \\ &\quad + \frac{1}{\sqrt{2}}(\mathcal{E}^{[x']}(\omega)\,\mathrm{e}^{\mathrm{i}\phi^{[x']}(\omega)} - \mathrm{i}\mathcal{E}^{[y']}(\omega)\,\mathrm{e}^{\mathrm{i}\phi^{[y']}(\omega)})\hat{\mathbf{L}} \\ &= \mathcal{E}^{[R]}(\omega)\,\mathrm{e}^{\mathrm{i}\phi^{[R]}(\omega)}\hat{\mathbf{R}} + \mathcal{E}^{[L]}(\omega)\,\mathrm{e}^{\mathrm{i}\phi^{[L]}(\omega)}\hat{\mathbf{L}}\end{aligned} \tag{14}$$

where $\mathcal{E}^{[R]}(\omega)$ and $\mathcal{E}^{[L]}(\omega)$ are the *dextrogyre* and *levogyre* amplitudes and $\phi^{[R]}(\omega)$ and $\phi^{[L]}(\omega)$ are the corresponding phases.

For polarization-resolved THz-TDS the electric field of a terahertz pulse is recorded as a reference, then the sample is placed in the terahertz path and the electric field is recorded again just like in 'traditional' TDS. Let $E^{[u]}_{\mathrm{ref}}(\omega) = \mathcal{E}^{[u]}_{\mathrm{ref}}(\omega)\,\mathrm{e}^{\mathrm{i}\phi^{[u]}_{\mathrm{ref}}(\omega)}$ and $E^{[u]}_{\mathrm{sam}}(\omega) = \mathcal{E}^{[u]}_{\mathrm{sam}}(\omega)\,\mathrm{e}^{\mathrm{i}\phi^{[u]}_{\mathrm{sam}}(\omega)}$ be the (Fourier transformed) electric fields measured for reference and sample respectively 'projected' in the arbitrary polarization state u, the complex transmittance is given by

$$\tilde{T}^{[u]} = \frac{E^{[u]}_{\mathrm{sam}}(\omega)}{E^{[u]}_{\mathrm{ref}}(\omega)} = \frac{\mathcal{E}^{[u]}_{\mathrm{sam}}(\omega)}{\mathcal{E}^{[u]}_{\mathrm{ref}}(\omega)}\,\mathrm{e}^{\mathrm{i}(\phi^{[u]}_{\mathrm{sam}}(\omega)-\phi^{[u]}_{\mathrm{ref}}(\omega))}. \tag{15}$$

Numerical methods can be used for the extraction of optical parameters from the measured transmittance [30] of arbitrary thickness; however, in this section the discussion will be restricted to the case of a free standing *optically thick* sample. If the propagation delay time of a pulse in the crystal is much larger than the duration of the pulse it is possible to avoid the overlapping of the terahertz pulse with its own internal reflections in the sample during measurement. This allows the Fabry–Perot term to be neglected (see [31]) and analytical determination of both the real

$$n^{[u]}(\omega) = 1 + \frac{c}{\omega d}(\phi^{[u]}_{\mathrm{sam}}(\omega) - \phi^{[u]}_{\mathrm{ref}}(\omega)) \tag{16}$$

and the imaginary

$$\kappa^{[u]}(\omega) = \frac{c}{2\omega d}\ln\left[\frac{\mathcal{E}^{[u]}_{\mathrm{sam}}(\omega)/\mathcal{E}^{[u]}_{\mathrm{ref}}(\omega)}{t^{[u]}_{12}(\omega)t^{[u]}_{21}(\omega)}\right] \tag{17}$$

parts of the refractive index, where d is the sample thickness, $t^{[u]}_{12}(\omega) = 2/(\tilde{n}^{[u]}(\omega)+1)$ and $t_{21}(\omega) = 2\tilde{n}^{[u]}(\omega)/(\tilde{n}^{[u]}(\omega)+1)$ are the Fresnel transmission coefficients at the surfaces of the sample. The absorption coefficient is given by $\alpha^{[u]}(\omega) = 2\omega\kappa^{[u]}(\omega)/c$.

3.1. Birefringence

Birefringence is a well known phenomenon that consists of the existence of two propagation speeds for electromagnetic radiation and is defined as the difference of refractive indices of the two eigenwaves. Let $\hat{\mathbf{O}}$ and $\hat{\mathbf{E}}$ be the unit Jones vectors parallel to the ordinary and extraordinary axes, respectively. In this case the birefringence is defined as $\delta n(\omega) = n^{[E]}(\omega) - n^{[O]}(\omega)$, therefore

$$\delta n(\omega) = \frac{c}{\omega d}\left[\phi^{[E]}_{\mathrm{sam}}(\omega) - \phi^{[E]}_{\mathrm{ref}}(\omega) - \phi^{[O]}_{\mathrm{sam}}(\omega) + \phi^{[O]}_{\mathrm{ref}}(\omega)\right]. \tag{18}$$

In order to facilitate the analysis, the axes of the crystal can be aligned with the directions corresponding to $\hat{\mathbf{H}}$ and $\hat{\mathbf{V}}$, avoiding the need to reexpress the experimentally acquired data in a different base.

3.2. Optical activity

Optical activity is another characteristic exhibited by various media, in which the angle of polarization of a linearly polarized wave changes as the wave propagates through the crystal. Optical activity is a form of birefringence in which the two different propagation speeds of the eigenwaves correspond to the dextrogyre and levogyre states, in contrast to the linearly polarized states in 'traditional' birefringence. The rotatory power ρ, defined as the angle of rotation of the plane polarized

wave by length unit, is commonly used to quantify optical activity

$$\rho(\omega) = \frac{\omega}{2c}\left(n^{[L]}(\omega) - n^{[R]}(\omega)\right) = \frac{1}{2d}[\phi^{[L]}_{\text{sam}}(\omega) - \phi^{[L]}_{\text{ref}}(\omega) - \phi^{[R]}_{\text{sam}}(\omega) + \phi^{[R]}_{\text{ref}}(\omega)]. \tag{19}$$

3.3. Linear dichroism

Dichroism is defined as the difference in absorption of electromagnetic radiation in a medium depending on its polarization state. For example a wire-grid polarizer filter is a highly dichroic optical element, which absorbs/reflects radiation heavily in one plane of polarization while being almost transparent in the orthogonal direction. Mathematically it can be expressed as

$$\mathcal{LD}(\omega) = \alpha^{[E]}(\omega) - \alpha^{[O]}(\omega) = \frac{1}{d}\ln\left[\frac{t^{[O]}_{12}(\omega)t^{[O]}_{21}(\omega)}{t^{[E]}_{12}(\omega)t^{[E]}_{21}(\omega)}\frac{\mathcal{E}^{[E]}_{\text{sam}}(\omega)\mathcal{E}^{[O]}_{\text{ref}}(\omega)}{\mathcal{E}^{[E]}_{\text{ref}}(\omega)\mathcal{E}^{[O]}_{\text{sam}}(\omega)}\right]. \tag{20}$$

3.4. Circular dichroism

Circular dichroism is the different absorption of dextrogyre and levogyre radiation given by

$$\mathcal{CD}(\omega) = \alpha^{[R]}(\omega) - \alpha^{[L]}(\omega) = \frac{1}{d}\ln\left[\frac{t^{[L]}_{12}(\omega)t^{[L]}_{21}(\omega)}{t^{[R]}_{12}(\omega)t^{[R]}_{21}(\omega)}\frac{\mathcal{E}^{[R]}_{\text{sam}}(\omega)\mathcal{E}^{[L]}_{\text{ref}}(\omega)}{\mathcal{E}^{[R]}_{\text{ref}}(\omega)\mathcal{E}^{[L]}_{\text{sam}}(\omega)}\right]. \tag{21}$$

Circular dichroism is of particular interest in biochemistry. Large biomolecules such as proteins and nucleic acids present low-frequency (terahertz) vibrational resonances related to their structure and function [32]; given the chiral nature of these systems they present different absorption cross sections for levogyre and dextrogyre states. Therefore terahertz circular dichroism spectroscopy has the potential to provide a powerful tool in this field [33].

Depending on the particular material under study it is common to find combinations of dielectric and absorptive effects. For instance birefringence and linear dichroism or optical activity and circular dichroism tend to appear in the same materials. In these cases it could be convenient to define the complex birefringence $\delta\tilde{n}(\omega) = \delta n(\omega) + \mathrm{i}c\,\mathcal{LD}(\omega)/2\omega$ and the complex optical activity $\tilde{\rho}(\omega) = 2c\,\rho(\omega)/\omega + \mathrm{i}c\,\mathcal{CD}(\omega)/2\omega$ which are anisotropic complex dielectric characteristics. It is important to point out that this method relies heavily on choosing the appropriate Jones vectors based on previous knowledge of the system being examined; an alternative approach can be found in [34].

4. Spectroscopy of birefringent materials

In this section two measurements of the birefringence of quartz are presented. The spectrometer used is described in detail in [27]. A mode-locked Ti:sapphire oscillator supplied 50 fs pulses with a repetition rate of ∼80 MHz and average power ∼400 mW. About 70% of the power was split and used to excite a 3 mm thick, 400 μm gap semi-insulating GaAs terahertz photoconductive emitter biased with a square wave (±100 V, ∼ 21 kHz). The remaining laser power was used to gate a three-contact photoconductive detector [19] connected to two lock-in amplifiers referenced to the emitter's bias frequency. The emitter was aligned at an angle of 0° (horizontally) for the first experiment and at 45° for the second one in order to produce terahertz pulses with plane polarization at those angles. A 10.54 mm thick X-cut quartz crystal was placed in such a way that its Y (ordinary) and Z (extraordinary) axes were aligned on the ±45° directions in the first experiment and on the horizontal and vertical directions for the second experiment. The reference electric field $\mathbf{E}_{\text{ref}}$ was measured before mounting the sample (figures 2(a) and (c)), then the electric field $\mathbf{E}_{\text{sam}}$ with the quartz sample in the terahertz path was also measured (figures 2(b) and (d)). Substantial differences can be noticed between $\mathbf{E}_{\text{ref}}$ and $\mathbf{E}_{\text{sam}}$. There is a delay of ∼40 ps between the two waves due to the delay caused by the optical density of the quartz sample. Also the total amplitude of the wave is considerably smaller, caused by the Fresnel transmission at the two faces of the quartz sample. Additionally an important difference in the shape of the wave may be observed: the original transient became split into two linearly polarized transients as it propagated through the medium, one with the electric field parallel to the optical axis and one perpendicular. These ordinary and extraordinary components are separated by ∼1.7 ps in both cases from each other after traversing the sample.

Initially the quartz sample was aligned with the ordinary and extraordinary axes at ±45° and the corresponding time-domain spectra were acquired. In order to analyse this case it was necessary to reexpress the data on the basis of the plane polarized states at ±45°. Subsequently the quartz sample was aligned with the ordinary and extraordinary axes in the horizontal and vertical directions, and therefore the data, in this case, were measured directly in the appropriate base for their analysis. The refractive indices can be obtained by applying equation (16) to the electric fields $E^{[H,V]}_{\text{ref}}$ and $E^{[H,V]}_{\text{sam}}$. The two refractive indices obtained are shown in figures 3(a) and (c) (respectively, for the two experimental geometries). Both pairs of curves shown in figures 3(a) and (c) match very well with each other and with values reported [35] which were measured separately for the ordinary and extraordinary refraction indices. When comparing the two methods there are two main differences. Firstly the separate characterization of the components makes the data acquisition time at least twice as long. Secondly, and most importantly, the physical rotation of the terahertz electric field detector can introduce slight misalignments that can, in time, produce changes in the actual response of the detector as well as additional shifts of the relative phase that have as a consequence 'artificial' changes in the refractive indices.

5. Conclusions

The generalized equations for extracting the anisotropic complex dielectric properties of materials from THz-TDS data have been presented. The particular cases of birefringence,

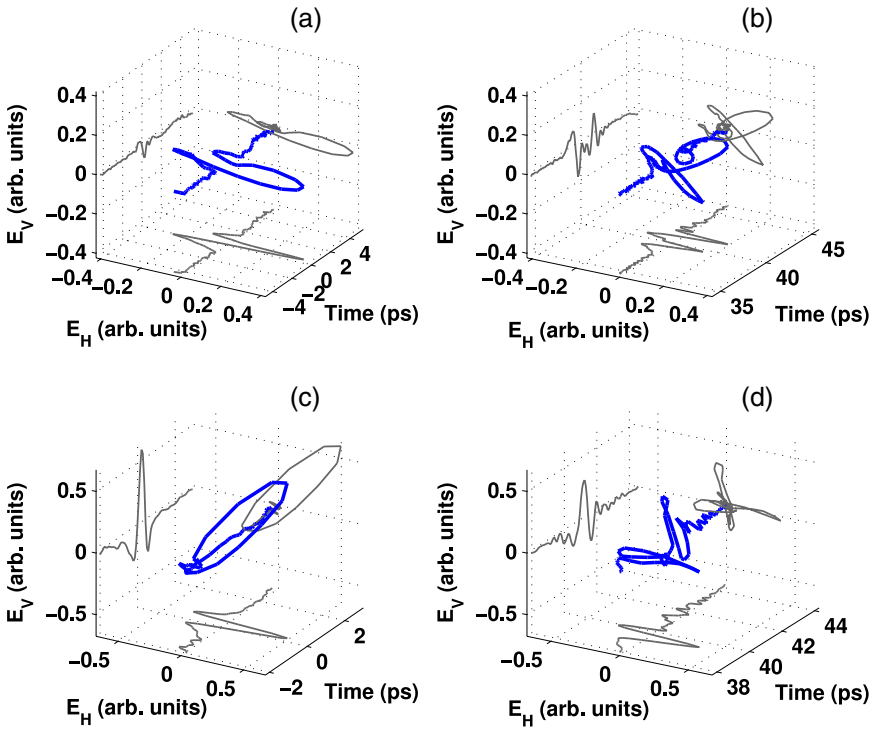

Figure 2. Three-dimensional representations of the measured time-domain data; the curves in grey are the projections on each of the planes. (a) Reference electric field horizontally polarized. (b) Same as (a) after propagating through a 10.54 mm sample of X-cut quartz with the ordinary and extraordinary axes at ±45°. (c) Reference polarized at 45°. (d) Same as (c) after propagating through the same quartz sample with the ordinary and extraordinary axes in horizontal and vertical directions.

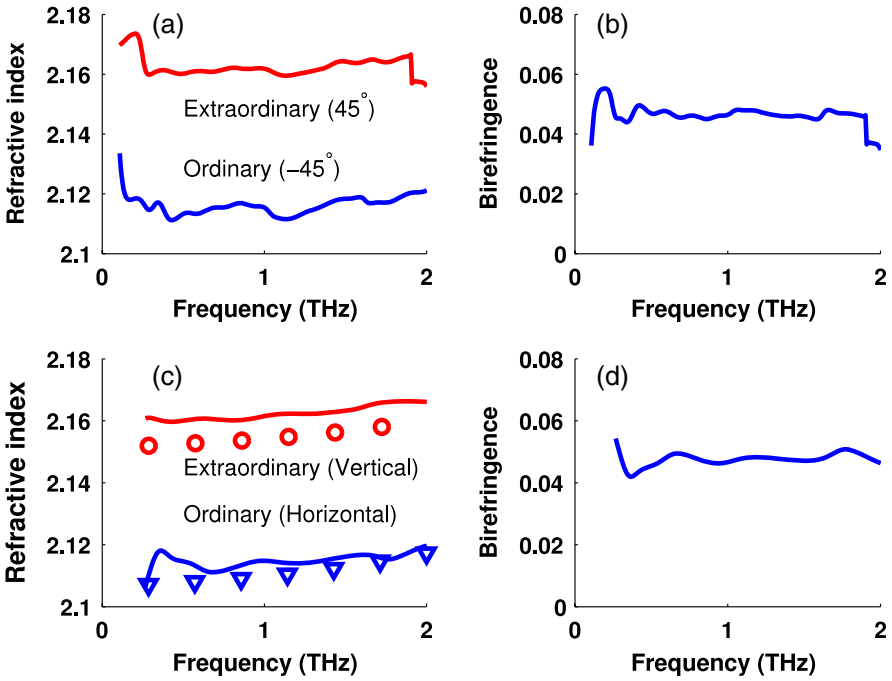

Figure 3. (a) Ordinary and extraordinary refractive indices of quartz measured by polarization-resolved THz-TDS with the crystal axes at ±45°. (b) Birefringence of quartz calculated from (a). (c) Refractive indices of quartz extracted from data taken with the crystal axes in the horizontal and vertical directions; circles and triangles are reported values from [35]. (d) Birefringence of quartz calculated from (c).

optical activity, linear and circular dichroism were discussed in more detail owing to their importance in the fields of physics and chemistry. Two experiments measuring birefringence of quartz were presented, demonstrating the validity of the equations and the importance of choice of the Jones vector as the basis for the analysis of the data.

Acknowledgments

The authors would like to thank the EPSRC (UK) and the Royal Society for financial support of this work.

References

[1] Auston D H, Cheung K P and Smith P R 1984 Picosecond photoconducting hertzian dipoles *Appl. Phys. Lett.* **45** 284
[2] Auston D H and Cheung K P 1985 Coherent time-domain far-infrared spectroscopy *J. Opt. Soc. Am.* B **2** 606–12
[3] Hu B B, Zhang X C, Auston D H and Smith P R 1990 Free-space radiation from electro-optic crystals *Appl. Phys. Lett.* **56** 506–8
[4] Auston D H and Nuss M C 1988 Electrooptic generation and detection of femtosecond electrical transients *IEEE J. Quantum Electron.* **24** 184
[5] Wu Q and Zhang X C 1995 Free-space electrooptic sampling of terahertz beams *Appl. Phys. Lett.* **67** 3523–5
[6] Schmuttenmaer C A 2004 Exploring dynamics in the far-infrared with terahertz spectroscopy *Chem. Rev.* **104** 1759–79
[7] Chamberlain J M 2004 Where optics meets electronics: recent progress in decreasing the terahertz gap *Phil. Trans. R. Soc.* A **362** 199–211
[8] Malevich V L 2002 Monte Carlo simulation of THz-pulse generation from semiconductor surface *Semicond. Sci. Technol.* **17** 551
[9] Johnston M B, Whittaker D M, Corchia A, Davies A G and Linfield E H 2002 Simulation of terahertz generation at semiconductor surfaces *Phys. Rev.* B **65** 165301
[10] Castro-Camus E, Lloyd-Hughes J and Johnston M B 2005 Three-dimensional carrier-dynamics simulation of terahertz emission from photoconductive switches *Phys. Rev.* B **71** 195301
[11] Lloyd-Hughes J, Castro-Camus E, Fraser M D, Jagadish C and Johnston M B 2004 Carrier dynamics in ion-implanted GaAs studied by simulation and observation of terahertz emission *Phys. Rev.* B **70** 235330
[12] Lloyd-Hughes J, Castro-Camus E and Johnston M B 2005 Simulation and optimisation of terahertz emission from ingaas and inp photoconductive switches *Solid State Commun.* **136** 595–600
[13] Shen Y C, Upadhya P C, Linfield E H, Beere H E and Davies A G 2003 Ultrabroadband terahertz radiation from low-temperature-grown GaAs photoconductive emitters *Appl. Phys. Lett.* **83** 3117–9
[14] Tani M, Sakai K and Mimura H 1997 Ultrafast photoconductive detectors based on semi-insulating GaAs and InP *Japan. J. Appl. Phys.* 2 **36** L1175–8
[15] Kono S, Tani M, Gu P and Sakai K 2000 Detection of up to 20 THz with a low-temperature-grown GaAs photoconductive antenna gated with 15 fs light pulses *Appl. Phys. Lett.* **77** 4104
[16] Liu T A, Tani M, Nakajima M, Hangyo M and Pan C L 2003 Ultrabroadband terahertz field detection by photoconductive antennas based on multi-energy arsenic-ion-implanted GaAs and semi-insulating GaAs *Appl. Phys. Lett.* **83** 1322–4
[17] Liu T A, Tani M, Nakajima M, Hangyo M, Sakai K, Nakashima S and Pan C L 2004 Ultrabroadband terahertz field detection by proton-bombarded InP photoconductive antennas *Opt. Express* **12** 2954–9
[18] Castro-Camus E, Fu L, Lloyd-Hughes J, Tan H H, Jagadish C and Johnston M B 2008 Photoconductive response correction for detectors of terahertz radiation *J. Appl. Phys.* **104** 053113
[19] Castro-Camus E, Lloyd-Hughes J, Johnston M B, Fraser M D, Tan H H and Jagadish C 2005 Polarization-sensitive terahertz detection by multicontact photoconductive receivers *Appl. Phys. Lett.* **86** 254102
[20] Makabe H, Hirota Y, Tani M and Hangyo M 2007 Polarization state measurement of terahertz electromagnetic radiation by three-contact photoconductive antenna *Opt. Express* **15** 11650–7
[21] Hussain A and Andrews S R 2008 Ultrabroadband polarization analysis of terahertz pulses *Opt. Express* **16** 7251–7
[22] Masson J B and Gallot G 2006 Terahertz achromatic quarter-wave plate *Opt. Lett.* **31** 265–7
[23] Hirota Y, Hattori R, Tani M and Hangyo M 2006 Polarization modulation of terahertz electromagnetic radiation by four-contact photoconductive antenna *Opt. Express* **14** 4486–93
[24] Awasthi S K, Srivastava A, Malaviya U and Ojha S P 2008 Wide-angle, broadband plate polarizer in terahertz frequency region *Solid State Commun.* **146** 506–9
[25] Peralta X G, Smirnova E I, Azad A K, Chen H T, Taylor A J, Brener I and O'Hara J F 2009 Metamaterials for Thz polarimetric devices *Opt. Express* **17** 773–83
[26] Xu J, Ramian G J, Galan J F, Savvidis P G, Scopatz A M, Birge R R, Allen J and Plaxco K W 2003 Terahertz circular dichroism spectroscopy: a potential approach to the *in situ* detection of life's metabolic and genetic machinery *Astrobiology* **3** 489–504
[27] Castro-Camus E, Lloyd-Hughes J, Fu L, Tan H H, Jagadish C and Johnston M B 2007 An ion-implanted InP receiver for polarization resolved terahertz spectroscopy *Opt. Express* **15** 7047–57
[28] Born M and Wolf E 1999 *Principles of Optics* (Cambridge: Cambridge Univeristy Press)
[29] Yariv A and Yeh P 2003 *Optical Waves in Crystals: Propagation and Control of Laser Radiation* (New York: Wiley Inter-science)
[30] Duvillaret L, Garet F and Coutaz J L 1999 Highly precise determination of optical constants and sample thickness in terahertz time-domain spectroscopy *Appl. Opt.* **38** 409–15
[31] Duvillaret L, Garet F and Coutaz J L 1996 A reliable method for extraction of material parameters in terahertztime-domain spectroscopy *IEEE J. Sel. Top. Quantum Electron.* **2** 739–46
[32] Castro-Camus E and Johnston M B 2008 Conformational changes of photoactive yellow protein monitored by terahertz spectroscopy *Chem. Phys. Lett.* **455** 289–92
[33] Xu J, Galan J, Ramian G, Savvidis P, Scopatz A, Birge R R, Allen S J and Plaxco K 2003 Terahertz circular dichroism spectroscopy of biomolecules *Proc. Soc. Photo-Opt. Instrum. Eng.* **5268** 19–26
[34] Savenkov S N, Marienko V V, Oberemok E A and Sydoruk O 2006 Generalized matrix equivalence theorem for polarization theory *Phys. Rev.* E **74** 056607
[35] Grischkowsky D, Keiding S, van Exter M and Fattinger Ch 1990 Far-infrared time-domain spectroscopy with terahertz beams of dielectrics and semiconductors *J. Opt. Soc. Am.* B **7** 2006–15